Coarsening dynamics of the XY model

B. Yurke, A. N. Pargellis, T. Kovacs, and D. A. Huse
AT&T Bell Laboratories, Murray Hill, New Jersey 07974
(Received 20 October 1992)

It is the conventional wisdom that the correlation length for the XY model with linear damping should asymptotically grow diffusively as the square root of time after a quench into the ordered phase. This implies that the defect density ρ should decay with time as $\rho \propto t^{-\nu}$ with the scaling exponent $\nu=1$. We present evidence, by numerically integrating the equations of motion for a two-dimensional XY model, for a logarithmic correction to this scaling which makes it difficult to reach the asymptotic regime $\nu=-d(\ln\rho)/d(\ln t)=1$. Even after the defect density has decayed by three orders of magnitude $\nu=0.91$, which still deviates by 10% from the asymptotic value.

PACS number(s): 64.60.Cn

There is considerable interest in the dynamics of the defects produced during a symmetry-breaking phase transition [1,2]. One such system is the planar, time-dependent Ginzburg-Landau model having SO(2) symmetry. The planar XY model, which describes the dynamics of spins lying in the xy plane, is a discretized approximation of this Ginzburg-Landau model. When the system is quenched from the high-temperature, disordered phase to the low-temperature, ordered phase the continuous symmetry SO(2) of the high-temperature phase is broken to the Z_1 symmetry of the low-temperature phase [3,4]. The topological defects generated in this temperature quench are of codimension two (thus pointlike for the two-dimensional system studied below) and have integral winding numbers. If the spins are allowed to relax via linear damping from an initially random configuration one expects the system to anneal diffusively, and the correlation length ξ to grow as the square root of time [5,6]. This implies that the defect density ρ should scale as $\rho \sim \xi^{-2} \sim t^{-\nu}$ where $\nu=1$. Several numerical studies have been done which purport to have seen this scaling [5,7]. We report on numerical studies which cover more decades in time than previous studies. We present evidence for a logarithmic correction to the scaling which suggests that the system approaches $\nu=1$ scaling very slowly. Even after the defect density has decayed by three orders of magnitude the scaling exponent, defined as $\nu=-d(\ln\rho)/d\ln t$), has only increased from 0.75 to 0.91, still 10% short of the asymptotic scaling $\nu=1$.

Before presenting our numerical work we present an argument for the expected coarsening behavior for the time-dependent Ginzburg-Landau model. The time-dependent Ginzburg-Landau model with a vector order parameter $\mathbf{n}=(n_x,n_y)$ has the form

$$\gamma\frac{\partial \mathbf{n}}{\partial t}=\frac{\delta \mathcal{F}}{\delta \mathbf{n}}+\boldsymbol{\eta}\ , \tag{1}$$

where γ is the damping constant (assumed to be real and positive). $\boldsymbol{\eta}$ is Gaussian white noise having zero mean and, according to the fluctuation-dissipation theorem, the moments

$$\langle \eta_i(\mathbf{r},t)\eta_j(\mathbf{r}',t')\rangle = 2k_B T\gamma\delta_{i,j}\delta(\mathbf{r}-\mathbf{r}')\delta(t-t')\ , \tag{2}$$

where T is the equilibrium temperature. We take the free energy to have the form

$$\mathcal{F}=\int d\mathbf{r}\left[\frac{\kappa}{2}(\partial_\alpha n_\beta)^2+\frac{\lambda}{4}(\mathbf{n}^2-1)^2\right]\ , \tag{3}$$

where κ is an elastic constant, λ is the strength of the nonlinearity that drives $\mathbf{n}$ towards unit length, and it is understood that the indices α and β are summed over following the Einstein convention of summing over repeated indices. The field equation (equation of motion) generated by substituting Eq. (2) into Eq. (1) is

$$\gamma\frac{\partial \mathbf{n}}{\partial t}=\kappa\nabla^2\mathbf{n}-\lambda(\mathbf{n}^2-1)\mathbf{n}+\boldsymbol{\eta}\ . \tag{4}$$

In the following analysis we initially consider the $T=0$ case, where the Langevin noise is zero. Equation (4) has time-independent solutions of the form

$$\mathbf{n}=n(r)[\cos(s\phi)\mathbf{i}+\sin(s\phi)\mathbf{j}]\ , \tag{5}$$

where $\mathbf{i}$ and $\mathbf{j}$ are Cartesian unit vectors, the winding number s takes on integer values, and r and ϕ are the usual polar coordinate variables, $r=(x^2+y^2)^{1/2}$ and $\phi=\tan^{-1}(y/x)$. The length $n(r)$ of the vector $\mathbf{n}$ approaches unity for large r and goes to zero as r goes to zero. The length scale, or core radius R_c, at which $n(r)$ crosses over from zero to one is set by the parameter λ in the second term on the right-hand side of Eq. (3). These are the solutions for an isolated topological defect. The energy of a topological defect grows logarithmically with its size and to a good approximation is given by

$$\mathcal{E}=\pi s^2\kappa\ln(R/R_c)\ , \tag{6}$$

where R is the size of the topological defect. This is the distance to the boundary for the case of an isolated defect or the distance beyond which the strain field of the defect is shielded due to the presence of other defects.

We first consider the case of an isolated pair of defects. The attractive force F_a between two defects of opposite winding number, i.e., s and $-s$, is [8]

$$F_a=-2\pi s^2\kappa/D\ , \tag{7}$$

where D is the separation between defects. The time dependence described by Eq. (1) is viscous relaxation (we are taking γ to be real). Consequently all forces arising from gradients in the free-energy density will be opposed by a frictional force of equal magnitude. The friction force depends logarithmically [9–13] on the defect size R,

$$F_\mu = \mu \ln(R/R_c) v \ , \tag{8}$$

where $v = dD/dt$ is the magnitude of the velocity of the defect and μ is proportional to γ. This shows the mobility $\Gamma = v/F$ depends logarithmically on defect size as $\Gamma \propto (\ln R)^{-1}$. For two coalescing defects, $D \sim R$, giving for the equation of motion

$$2\mu \ln\left[\frac{D}{R_c}\right]\frac{dD}{dt} = -\frac{2\pi s^2 \kappa}{D} \ , \tag{9}$$

which is integrated by parts to give

$$D^2\left[\ln\left[\frac{D}{R_c}\right] - \frac{1}{2}\right] = \frac{2\pi s^2 \kappa}{\mu}(t_0 - t) \ , \tag{10}$$

where t_0 is the time of annihilation.

The above expressions for the viscous and elastic forces acting on a defect are used in the standard scaling argument to obtain an expression for the growth of the correlation length ξ, where $\xi \sim R \sim D$, with time when the system starts out with an initially random vector field $\mathbf{n}$ [14,15]. We need only consider defects with winding number $s = \pm 1$ since defects with higher winding number are unstable, decaying to defects of winding number $|s| = 1$. If the system is at all times characterized by the single length scale ξ then Eq. (7) gives, for the magnitude of the characteristic elastic force, $F_a \propto \kappa/\xi$. Similarly, since $v = d\xi/dt$ is the characteristic velocity, Eq. (8) gives, for the magnitude of the characteristic viscous force, $F_\mu \propto \mu \ln(\xi/R_c) d\xi/dt$. Equating the characteristic elastic force with the characteristic viscous force, and rearranging terms, gives the following differential equation:

$$\xi \frac{d\xi}{dt} = \frac{A\kappa/\mu}{\ln(\xi/R_c)} \ , \tag{11}$$

where A is the constant, of order unity, containing the geometric factors needed to make the proportionalities equalities. For large ξ, $\ln(\xi/R_c)$ varies very slowly with time and Eq. (11) has the form $d\xi/dt \propto 1/\xi$ with the scaling solution $\xi^2 \propto t$ expected for a system governed by a diffusion equation. Equation (11) can be integrated by parts to yield

$$\xi^2\left[\ln\left[\frac{\xi}{R_c}\right] - \frac{1}{2}\right] = \left[\frac{2A\kappa}{\mu}\right](t - t_0) \ , \tag{12}$$

where t_0 is an integration constant. Hence there are logarithmic corrections to the diffusive scaling behavior. In terms of the defect density $\rho = B/\xi^2$ and the "core density" $\rho_c = B/R_c^2$ this solution takes the form

$$\frac{\rho}{\ln(\rho_c/\rho) - 1} = \frac{B\mu/4A\kappa}{(t - t_0)} \ , \tag{13}$$

It is evident that the defect density should scale asymptotically as $\rho \sim t^{-1}$. The approach to this asymptotic regime is slow and may account for the $\rho \sim t^{-0.75}$ scaling observed at earlier times by previous workers [5,16] in numerical studies. The logarithmic correction is more easily seen by determining the time derivative of Eq. (13), which also eliminates the integration constant t_0. Rearranging terms gives

$$\frac{1}{\rho^2}\left[\frac{d\rho}{dt}\right] = \frac{4A\kappa/B\mu}{\ln(\rho/\rho_c)} \ . \tag{14}$$

The scaling argument used to generate Eqs. (11)–(14) employs only the two-body force between a pair of defects and the viscous force a defect experiences as it moves through the medium. It is conceivable that many-body effects could modify the asymptotic behavior of the coarsening dynamics. Here we provide numerical evidence to support the simple picture presented above. An example of the successful application of these scaling arguments to a two-dimensional system where the two-body interaction force and the friction force differ from Eq. (7) and Eq. (8), respectively, is given in Ref. [17].

In the XY model the phase ϕ_i at each lattice site i evolves according to

$$\gamma \frac{d\phi_i}{dt} = -\kappa \sum_j \sin(\phi_i - \phi_j) - \eta_i \ , \tag{15}$$

where η_i is the Langevin noise at site i. As for Eq. (2), the Langevin noise has zero mean and the moments

$$\langle \eta_i(t)\eta_j(t')\rangle = 2k_B\gamma\delta_{i,j}\delta(t - t') \ . \tag{16}$$

With the sum in Eq. (15) restricted to a neighborhood about each lattice site, the sum approximates the ∇^2 term appearing in Eq. (4). Therefore, the XY model is a discretized version of the Ginzburg-Landau model discussed above where the core radius of the defects is of the order of the lattice spacing. The numerical integration procedure employed by us for Eq. (15) is the Euler update [18],

$$\phi_i(t + \Delta t) = \phi_i(t) - \Delta t\left\{\eta_i(t) + \frac{\kappa}{\gamma}\sum_j \sin[\phi_i(t) - \phi_j(t)]\right\} \ . \tag{17}$$

The simulations were performed on a square lattice and the sum over j was carried out over the eight nearest neighbors of i. Periodic boundary conditions were imposed. We will report the time in number of time steps, or iterations, N, where $t = N\Delta t$ is the dimensionless time. At each site i the initial phase $\phi_i(0)$ was obtained from a random-number generator whose random numbers are uniformly distributed between 0 and 2π. The Langevin noise $\eta_i(t) = 2\pi c_L r_i$ consisted of random numbers r_i having a uniform distribution over the interval from -0.5 to 0.5. The constants κ and γ can be scaled away and were thus taken to be 1. The time step Δt was taken to be 0.05. No noticeable change was observed in the defect dynamics when $\Delta t = 0.005$. The order-to-disorder transition was determined to occur near $c_L \simeq 3$ where many

short-lived defect pairs begin to be created. For the runs reported here, $c_L=2$, giving the phase at a given lattice site an average kick of 9° for each time step. The runs were performed on a parallel processor containing 128×128 4-bit microprocessors (Model MP-1216D; MasPar Computer Corporation). A run out to $N=10^5$ iterations required 8 h of central processor time, making longer runs impractical.

Defect cores were identified by calculating the strain energy $\mathcal{E}_i$ at each site i,

$$\mathcal{E}_i=\sum_j[1-\cos(\phi_i-\phi_j)]\ . \tag{18}$$

If $\mathcal{E}_i$ was greater than 5 and if $\mathcal{E}_i$ was a local maximum at site i, the site was identified as a defect core. At early times, $N<30$, when the defect density is high this algorithm undercounts the number of defects by a factor of 2 when compared with other algorithms that determine the winding number about a site. For $N>100$ iterations this defect identification algorithm works reliably.

Following a standard imaging technique used to study thin free-standing films of smectic-C liquid crystals [8,19], in which the film is placed between two polarizers to make visible the topological defects, we found it useful to display the phase field ϕ_i as a Schlieren pattern. The pixel representing the site i was shaded using a gray scale that was proportional to $\sin^2(2\phi_i)$. Figure 1 shows a coarsening sequence displayed as a Schlieren pattern. Each frame is labeled with the time N in iterations (time steps). For this run a lattice of 512×512 was used and, for purposes of visual clarity, the Langevin noise amplitude was $c_L=1$. The defects appear as points from which four bright brushes emanate. Figure 2 shows the total number of defects ρ as a function of time (N) for various values of c_L. All runs were performed on a 1024×1024 lattice. The data shown for $c_L=2$ (filled circles) is the average of ten runs; the other curves are averaged over at least three runs each. For values of $c_L\le1.5$ there is pinning of the defects to lattice sites for $N>10^4$. For $c_L\ge2.8$ many short-lived defect pairs are generated. Therefore, the range $1.5<c_L<2.8$ allows sufficient Langevin noise to prevent the defects from pinning to the lattice, without generating significant numbers of defect pairs.

Figure 3 is a log-log plot of the number of defects versus time. The data shown are the average of ten runs with $c_L=2$ and a 1024×1024 lattice. The dashed line has a slope of -1, the expected diffusive scaling in the absence of any logarithmic corrections. This also makes visible the long-time curvature exhibited by the data when plotted on a log-log scale. It is our contention that this curvature is due to the logarithmic correction to the $\rho\propto t^{-1}$ scaling discussed in connection with Eq. (13). The solid curve is a fit of Eq. (13) to the numerical data with the fitting parameters given by $\rho_c=(4.28\pm0.30)\times10^6$ defects, $B\mu/4A\kappa=(2.24\pm0.02)\times10^5$ defect-iteration, and $t_0=0$. The core density ρ_c gives a defect core size of $R_c=0.495\pm0.018$ lattice units (l.u.), where $B=(1024\text{ l.u.})^2$. The data show Eq. (13) is able to adequately account for the long-time curvature with 0.91 ± 0.005 as the slope of the data during the last decade. One notes that at times before about 50 iterations there is a deviation from the scaling described in Eq. (13). We attribute this deviation of the data from the $\rho\ln\rho$ scaling to be due to discrete lattice effects where for more than 10^4 defects on a $(1024)^2$ lattice the average interdefect distance is less than 10 lattice units. We have observed this behavior in a variety of previous simulations, some employing hexagonal lattices and others con-

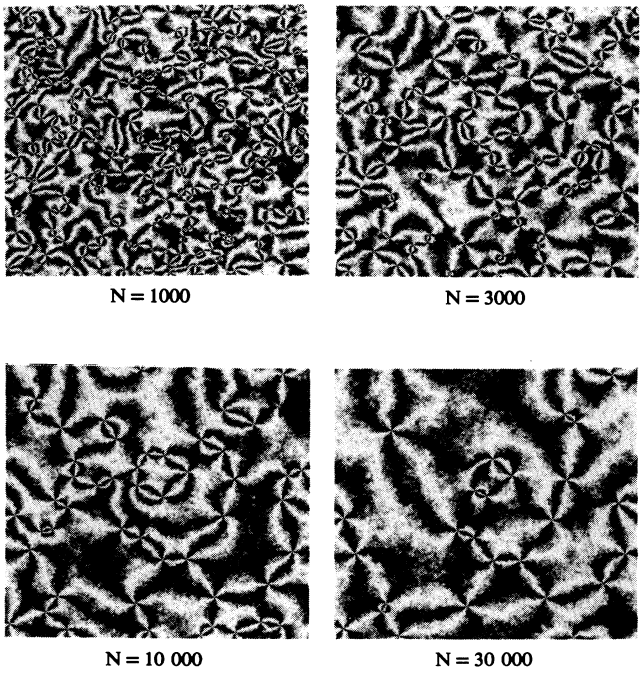

FIG. 1. A coarsening sequence of annihilating defects, shown as Schlieren patterns, with the gray scale proportional to $\sin^2(2\phi)$. The times in iterations after the initially random configuration label each frame. The Langevin noise was reduced to $c_L=1$ in this figure for visual clarity.

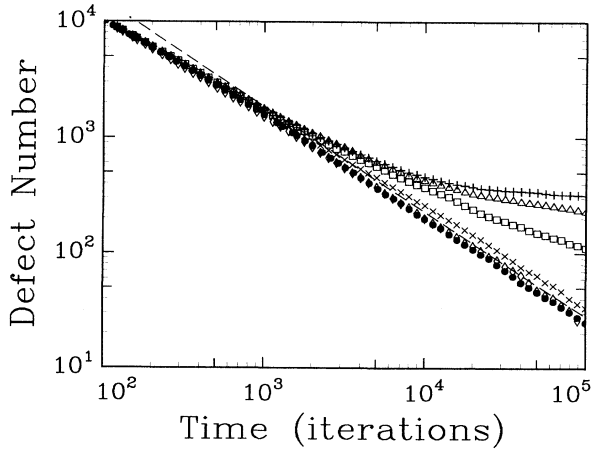

FIG. 2. Defect density vs time for various values of Langevin noise c_L. From top to bottom, $c_L=0,0.3,0.5,1,2,2.5$.

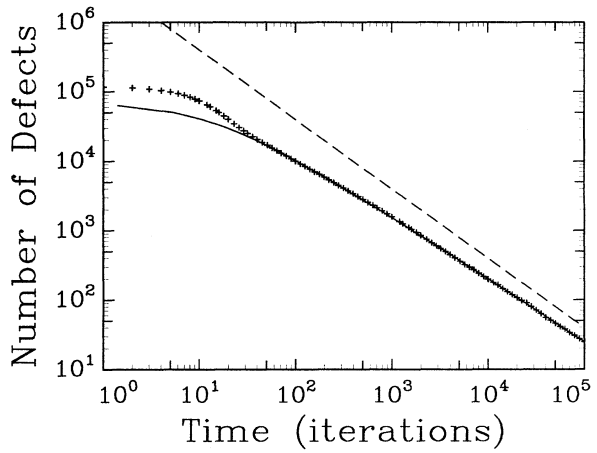

FIG. 3. Number of defects vs time since the quench, averaged over ten runs. The dashed line is the expected diffusive scaling $\rho \propto t^{-1}$ and the solid curve is a fit of Eq. (13) to the data, exhibiting the logarithmic correction to the scaling, $\rho \ln\rho \propto t^{-1}$.

sisting of discretized versions of Eq. (4) in which next-nearest neighbors were included in evaluating the gradient term and a λ term was included to give the defects a soft core. Consequently we believe our numerical results out to 10^5 iterations are robust and independent of the detailed algorithms employed. For $N < 30$ we observe an initial approach to scaling, probably due to the high defect density where the average interdefect distance is on the order of the core size R_c. For times $30 < N < 300$, $d\ln\rho/d\ln t \simeq -0.75$, similar to the initial, power-law scaling reported by Mondello and Goldenfeld [5]. However, our analysis, shown in Eq. (13), indicates this is a manifestation of $\rho\ln\rho \sim t^{-1}$ scaling which arises from the logarithmic dependence of defect mobility on defect size.

In order to more clearly see the logarithmic dependence we replot, in Fig. 4, the data shown in Fig. 3 as $-(1/\rho^2)(d\rho/dt)$ vs ρ. In the absence of logarithmic corrections $-(1/\rho^2)(d\rho/dt)$, the left-hand side of Eq. (14), would be constant and independent of ρ. The derivative $m = d\rho/dt$ is obtained by a least-squares fit of $\rho = mt + a$ to the data, by minimizing the vertical residuals in the neighborhood of the time t. This gives the result $d\rho/dt = [\langle \rho t\rangle - \langle\rho\rangle\langle t\rangle]/[\langle t^2\rangle - \langle t\rangle\langle t\rangle]$ where the averages are over five data points centered about the time t. The solid curve is a fit of Eq. (14) to the data, using the same value for ρ_c obtained when fitting to Eq. (13) and fitting over the same time interval, corresponding to values of $\rho \leq 10^4$. As expected, the value of $B\mu/4A\kappa = (2.34 \pm 0.02) \times 10^5$ is basically the same.

To demonstrate that the logarithmic correction to the scaling arises from the logarithmic dependence of the defect mobility on its size we studied the approach, and subsequent annihilation, of two point defects. The initial director field of the defect pair, with the $+1$ (-1) defect positioned at $y = 0$ and $x = a$ ($-a$), is specified by

$$\phi = \tan^{-1}\left[\frac{y}{x-a}\right] - \tan^{-1}\left[\frac{y}{x+a}\right] \tag{19}$$

at $t = 0$. Langevin noise is included with $c_L = 2$. Figure 5 is a sequence depicting the approach and annihilation of a pair of defects. Each frame is labeled with the time before time of annihilation and, as in Fig. 1, a 512×512 array was used with $c_L = 1$.

The interdefect separation distance D is plotted versus time before annihilation in Fig. 6 on a log-log scale. For

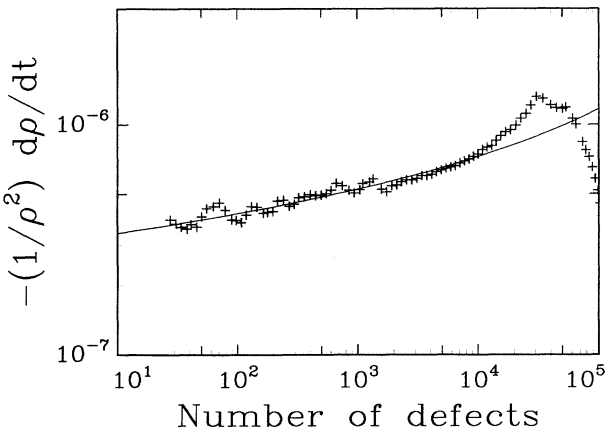

FIG. 4. The data of Fig. 2 replotted to more clearly show the logarithmic correction to the scaling of the defect density. The solid line is a fit of the results of the simulation to Eq. (14). In the absence of the $\ln\rho$ term the data would follow a straight, horizontal line.

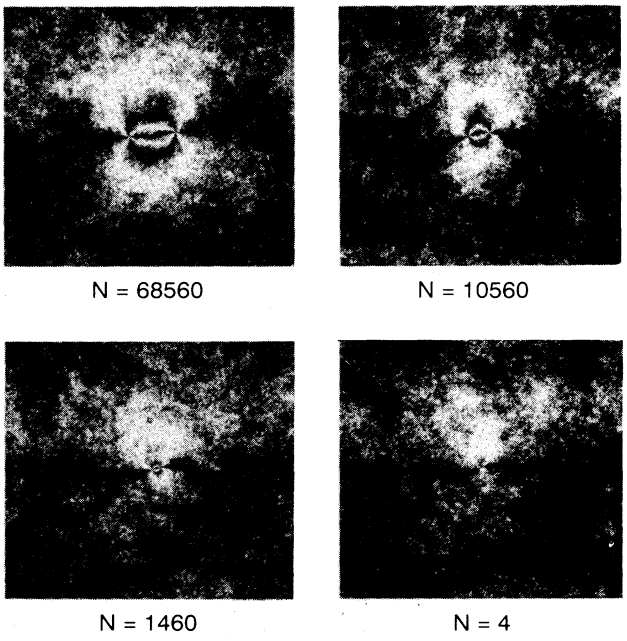

FIG. 5. A sequence showing the approach and final annihilation of a $+1$ and a -1 point defect. Each frame is labeled with the number of iterations before annihilation. For purposes of visual clarity the Langevin noise was set to $c_L = 1$ during this simulation.

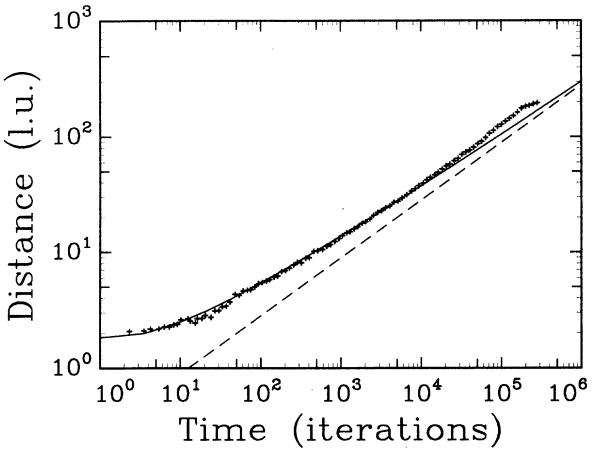

FIG. 6. The interdefect distance vs time for annihilating +1 and −1 point defects. The diffusive scaling $D^2 \propto t$ is shown by the dashed line. The solid curve is a fit of Eq. (10) to the data where $D^2 \ln D \propto t$ includes a logarithmic correction.

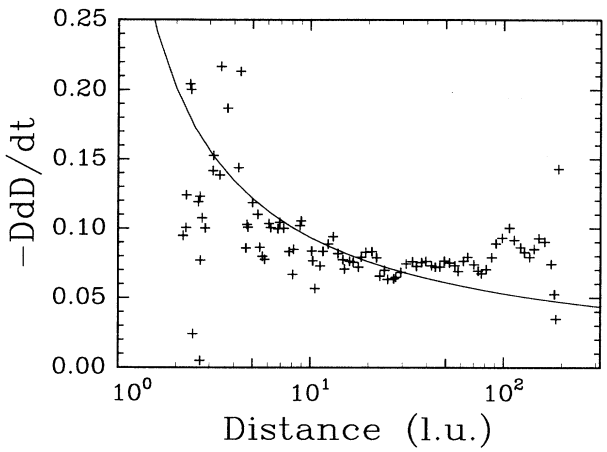

FIG. 7. The data of Fig. 5 replotted to show the deviation of $D\,dD/dt$ from a constant value due to logarithmic corrections. The solid curve is a fit of Eq. (9) to the data obtained from computer simulations.

each run, the annihilation time t_0 was chosen as the time (N_0 iterations) when the core identification algorithm, Eq. (18), first reported the presence of only one core. This time was typically $N_0 \sim 250\,000$ iterations. The data shown are an average of 20 runs using a 512×512 array and a Langevin noise of $c_L = 2$. The dashed line is the expected scaling for a diffusive system, $D \propto (t_0 - t)^{0.5}$. However, Fig. 6 shows the interdefect distance scales with time according to Eq. (10). The solid curve in Fig. 6 is a fit, over the time interval $30 < N_0 - N < 5 \times 10^4$ iterations, of Eq. (10) to the data. Data from the time interval $5 \times 10^4 < N_0 - N < 2 \times 10^5$ iterations, covering the beginning of the defect coalescence, were excluded from the fit because this data exhibited transient behavior where the periodicity of the boundary conditions caused the strain field to be greatly distorted by the "image pairs." This fit used the same core size, $R_c = 0.495$, as for the defect density analyses. The other two fitting parameters were $N_0' = 3$ (iterations) and $A\kappa/\mu = 0.269 \pm 0.004$ (l.u.^{2}/defect-iteration). The nonzero value of N_0' is a correction to our value of N_0 for the annihilation time, indicating our definition for the annihilation time differs by only three iterations from the time appropriate for Eq. (10). The value of $A\kappa/\mu = 0.269$ corresponds, with $B = (512$ l.u.$)^2$, to $B\mu/4A\kappa = (2.44 \pm 0.04) \times 10^5$, very close to the values previously obtained for defect coarsening. Following the same procedure as before with the coarsening of defects, in Fig. 7 we show the logarithmic correction more clearly by plotting $D\,dD/dt$ versus interdefect distance D. The solid curve is a fit of Eq. (9) to the data over the interval, $D = 3$–90 l.u., equivalent to the same time interval used in Fig. 6. As before, the core size is forced to be 0.495 l.u. The derivative dD/dt is obtained using the same procedure as that for the derivative $d\rho/dt$, discussed above. Minimizing the vertical residues gives, for the fitting parameter, $A\kappa/\mu = 0.281 \pm 0.008$, corresponding to $B\mu/4A\kappa = (2.32 \pm 0.07) \times 10^5$, which again is similar to the previously obtained values.

Our studies suggest that the transient $\rho \propto t^{-0.75}$ power-law scaling reported by Mondello and Goldenfeld [5] is actually due to the logarithmic dependence, $\Gamma \sim (\ln R)^{-1}$, of the defect mobility Γ on defect size R, resulting in the logarithmic scaling, $\rho \ln(\rho/\rho_c) \sim t^{-1}$. In the simulations presented here, performed on a MasPar computer, it was possible to carry out the simulations sufficiently far to detect curvature in $\log_{10}(\rho)$, for defect-density scaling. Simulations of the coalescence of a defect pair also show curvature in $\log_{10}(D)$, plotted as a function of $\log_{10}(t_0 - t)$, which is consistent with the scaling $D^2 \ln(D) \sim t_0 - t$ expected when the size dependence of the defect mobility is taken into account.

We gratefully acknowledge many fruitful discussions with Isaac Chuang.

[1] J. D. Gunton, M. San Miguel, and P. S. Sahni, in *Phase Transitions and Critical Phenomena,* edited by C. Domb and J. L. Lebowitz (Academic, London, 1983), p. 267.
[2] *Dynamics of Ordering Processes in Condensed Matter,* edited by S. Komura and H. Furukawa (Plenum, New York, 1988).
[3] N. D. Mermin, Rev. Mod. Phys. **51**, 591 (1979).
[4] J. M. Kosterlitz and D. J. Thouless, J. Phys. C **6**, 1181 (1973).
[5] M. Mondello and N. Goldenfeld, Phys. Rev. A **42**, 5865 (1990).
[6] H. Toyoki, Phys. Rev. A **42**, 911 (1990).
[7] R. Loft and T. A. DeGrand, Phys. Rev. B **35**, 8528 (1987).
[8] P. G. deGennes, *The Physics of Liquid Crystals* (Oxford University Press, London, 1974).
[9] C. D. Muzny and N. A. Clark, Phys. Rev. Lett. **68**, 804

(1992).
[10] H. Pleiner, Phys. Rev. A **37**, 3986 (1988).
[11] P. E. Cladis, W. van Saarloos, P. L. Finn, and A. R. Kortan, Phys. Rev. Lett. **58**, 222 (1987).
[12] G. Ryskin and M. Kremenetsky, Phys. Rev. Lett. **67**, 1574 (1991).
[13] A. Pargellis, N. Turok, and B. Yurke, Phys. Rev. Lett. **67**, 1570 (1991).
[14] I. M. Lifschitz, Zh. Eksp. Teor. Fiz. **42**, 1354 (1962) [Sov. Phys. JETP **15**, 939 (1962)].
[15] S. M. Allen and J. W. Cahn, Acta Metall. **27**, 1085 (1979).
[16] I. Chuang, Master's thesis, M. I. T., 1991.
[17] A. N. Pargellis *et al.*, Phys. Rev. A **46**, 7765 (1992).
[18] D. Potter, *Computational Physics* (Wiley, London, 1973), p. 37.
[19] S. Chandrasekhar, *Liquid Crystals* (Cambridge University Press, Cambridge, England, 1977).

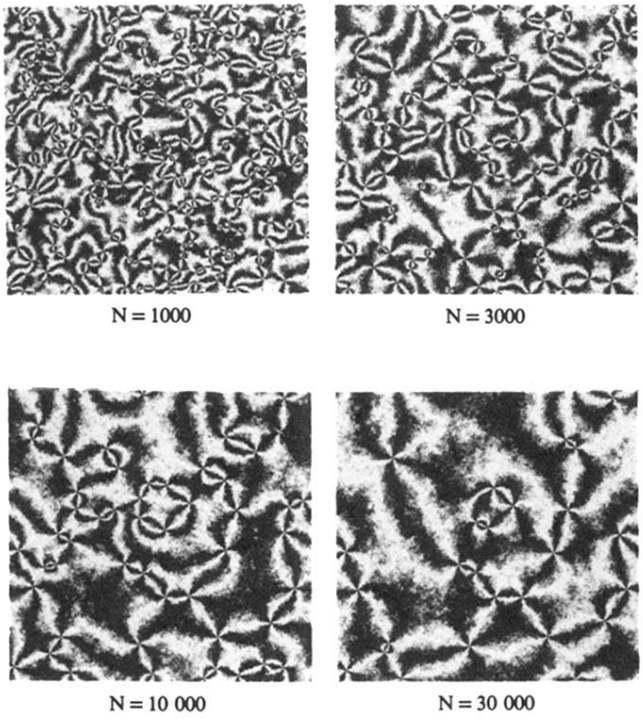

FIG. 1. A coarsening sequence of annihilating defects, shown as Schlieren patterns, with the gray scale proportional to $\sin^2(2\phi)$. The times in iterations after the initially random configuration label each frame. The Langevin noise was reduced to $c_L = 1$ in this figure for visual clarity.

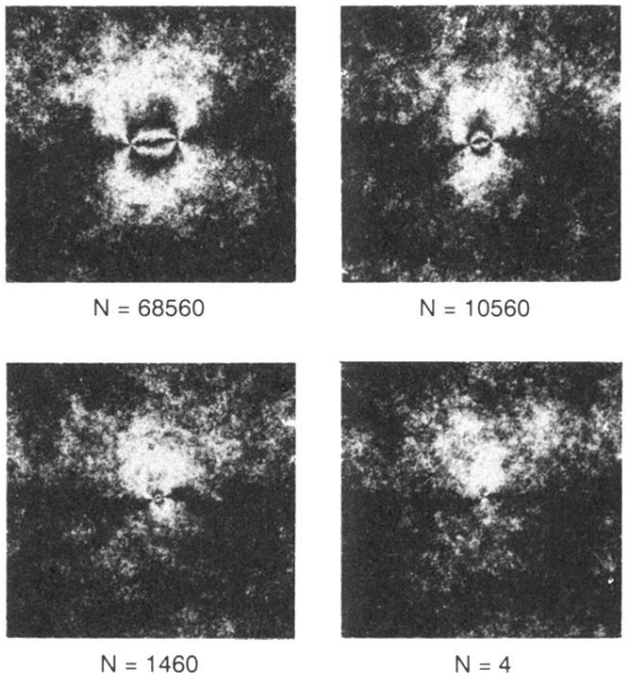

FIG. 5. A sequence showing the approach and final annihilation of a $+1$ and a -1 point defect. Each frame is labeled with the number of iterations before annihilation. For purposes of visual clarity the Langevin noise was set to $c_L = 1$ during this simulation.